

RESEARCH ARTICLE

Novel methods of imaging and analysis for the thermoregulatory sweat test

Michael S. Carroll,^{1,2} David W. Reed,² Nancy L. Kuntz,^{1,2} and Debra E. Weese-Mayer^{1,2}

¹Center for Autonomic Medicine in Pediatrics (CAMP), Ann & Robert H. Lurie Children's Hospital of Chicago and Stanley Manne Children's Research Institute, Chicago, Illinois; and ²Northwestern University Feinberg School of Medicine, Chicago, Illinois

Submitted 12 December 2017; accepted in final form 31 May 2018

Carroll MS, Reed DW, Kuntz NL, Weese-Mayer DE. Novel methods of imaging and analysis for the thermoregulatory sweat test. *J Appl Physiol* 125: 755–762, 2018. First published June 7, 2018; doi:10.1152/jappphysiol.01086.2017.—The thermoregulatory sweat test (TST) can be central to the identification and management of disorders affecting sudomotor function and small sensory and autonomic nerve fibers, but the cumbersome nature of the standard testing protocol has prevented its widespread adoption. A high-resolution, quantitative, clean and simple assay of sweating could significantly improve identification and management of these disorders. Images from 89 clinical TSTs were analyzed retrospectively using two novel techniques. First, using the standard indicator powder, skin surface sweat distributions were determined algorithmically for each patient. Second, a fundamentally novel method using thermal imaging of forced evaporative cooling was evaluated through comparison with the standard technique. Correlation and receiver operating characteristic analyses were used to determine the degree of match between these methods, and the potential limits of thermal imaging were examined through cumulative analysis of all studied patients. Algorithmic encoding of sweating and nonsweating regions produces a more objective analysis for clinical decision-making. Additionally, results from the forced cooling method correspond well with those from indicator powder imaging, with a correlation across spatial regions of -0.78 (confidence interval: -0.84 to -0.71). The method works similarly across body regions, and frame-by-frame analysis suggests the ability to identify sweating regions within ~ 1 s of imaging. Although algorithmic encoding can enhance the standard sweat testing protocol, thermal imaging with forced evaporative cooling can dramatically improve the TST by making it less time consuming and more patient friendly than the current approach.

NEW & NOTEWORTHY The thermoregulatory sweat test (TST) can be central to the identification and management of several common neurological disorders, but the cumbersome nature of the standard testing protocol has prevented its widespread adoption. In this study, images from 89 clinical TSTs were analyzed retrospectively using two novel techniques. Our results suggest that these improved methods could make sweat testing more reliable and acceptable for screening and management of a range of neurological disorders.

small fiber neuropathy; sudomotor; thermal imaging; thermoregulatory sweat test

INTRODUCTION

Sweating dysfunction impairs thermoregulatory control in humans. This may be secondary to primary dysfunction of

peripheral sweat glands but can also be an indicator of a small fiber neuropathy. Two standard methods are used to assess sudomotor function. One is Q-SWEAT, a quantitative measure of postganglionic sudomotor output dependent on local axon reflex stimulation of sweat glands. This method is relatively fast and well tolerated, but it only tests individual small anatomic regions and is not well suited to evaluating the most distal sites on the body (13). The second method is the thermoregulatory sweat test (TST), which assesses global distribution of sweating over the body surface with an indicator powder that changes from golden to purple in areas of sweating when subjects reach target warming in a humid chamber (13, 15, 22). TST reveals abnormalities of small sensory and autonomic nerve fiber function that cannot be assessed through standard sensory nerve conduction studies as performed in clinical neurophysiology laboratories. Furthermore, patterns of altered sweating can help identify distal neuropathies and localize pathology to affected spinal nerve roots or peripheral nerves (Fig. 1).

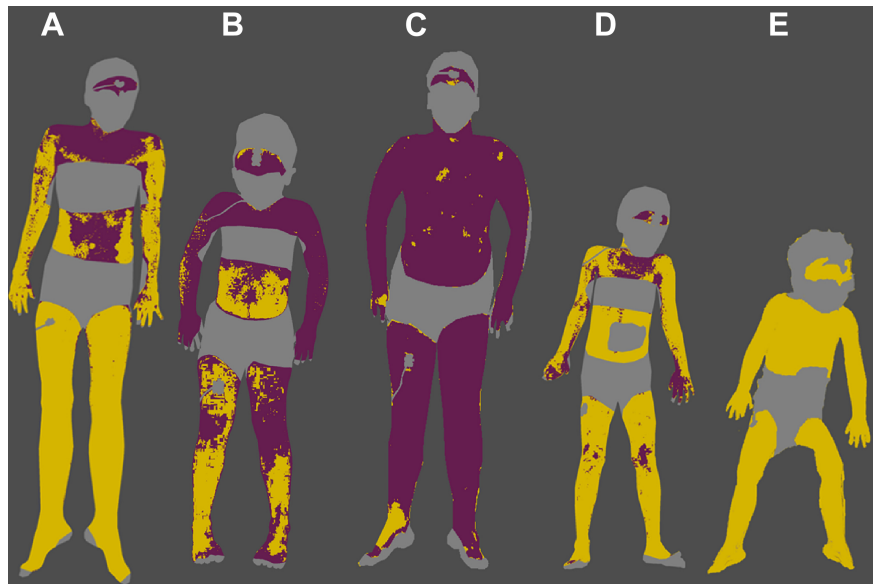
This article describes two improvements to standard TST methodology. The first uses a statistical classification method to partially automate the localization of sweating over the body surface when using the standard indicator powder. The second consists of using changes in skin temperature caused by forced evaporative cooling to detect body regions that sweat, an approach that could eliminate the use of the indicator powder. Skin areas that produce sweat show a rapid drop in temperature with evaporative cooling induced by fanning compared with those areas without sweat. The thermographic measurements reproduce the spatial resolution of powder-based visible light imaging with less mess and discomfort for the patient.

METHODS

The techniques described here were developed from the Ann & Robert H. Lurie Children's Hospital of Chicago clinical protocol for TST (which is based on the Mayo Clinic protocol) (13). Briefly, patients lie supine on a gurney outside of the testing chamber wearing disposable paper swimming trunks (and tube top for women), a paper head cover, eye goggles, and a face mask. Alizarin-based indicator powder is sprinkled on their skin, and skin surface and core temperature probes are placed. The patient and gurney are then rolled into a preheated custom-designed thermoregulatory chamber (built as a partnership between DMC, Inc. and Lurie Children's Hospital Center for Autonomic Medicine in Pediatrics). Sweating is induced with a protocol that raises core body temperature using a humid warming chamber and infrared heat lamps. Both ambient heat and humidity are controlled in the chamber. Additionally, overhead radiant heat lamps are used to provide additional heat, which gradually raises the patient's core body temperature during testing by at least 1°C or to 38°C ,

Address for reprint requests and other correspondence: M. S. Carroll, Center for Autonomic Medicine in Pediatrics (CAMP), Ann & Robert H. Lurie Children's Hospital of Chicago, 225 E. Chicago Ave., Box 165, Chicago, IL 60611-2605 (e-mail: mscarroll@luriechildrens.org).

Fig. 1. Representative clinical findings in thermoregulatory sweat testing. *A*: 13-yr-old girl with normal strength, muscle stretch reflexes, motor and sensory nerve conduction studies. She presented with neuropathic pain from a length-dependent small fiber peripheral neuropathy. *B*: 9-yr-old boy with orthostatic dizziness, gastrointestinal (GI) dysmotility, and assymmetric neuropathic pain (greater on the right lower extremity). He was diagnosed with seronegative autoimmune ganglionopathy. *C*: 14-yr-old boy with abdominal pain and GI dysmotility. TST results are normal except for focal anhidrosis around the medial right ankle at the site previous injury. *D*: 9-yr-old girl with GI dysmotility, abdominal pain, and 83% anhidrosis on TST. Peripheral nerve pathology was confirmed with results of Q-SWEAT volume on right extremities. *E*: 3-yr-old girl with global developmental delay, poor sleep, and unexplained fevers. A chromosomal microarray demonstrated a rare microdeletion associated with neurodevelopmental disorders. TST, thermoregulatory sweat test.



whichever is higher. Upon reaching this target core body temperature, well-hydrated individuals sweat over all exposed body surface regions. The presence of sweat gland abnormalities, autonomic dysfunction in control pathways for sweating (hypothalamus through peripheral autonomic fibers), and/or medications that inhibit sweating will produce TST abnormalities. The heat lamps are controlled by a custom servocontrol system taking inputs from the axillary and oral core temperature probes as well as the skin surface temperature probes. The system allows precise control over the rate of temperature increase as well as a failsafe mechanism that shuts down the heat lamps if temperature probes are disconnected or skin temperature rises beyond a safety threshold value.

Although the chamber and heating protocol are based on that developed at Mayo Clinic Rochester (13), the Lurie Children's Hospital TST was created with children in mind. There is extra space in the chamber for a caretaker or staff member to accompany the child during testing. The sides of the chamber are windowed to minimize potential for claustrophobia and allow visualization of an entertainment wall monitor. Standard videography and photography are used to record powder color change. At completion of standard testing, a handheld fan is used to rapidly return the patient to a more comfortable temperature. During cooling, a high-resolution ceiling-mounted infrared imaging camera documents skin surface temperature. After fan cooling, the patient is then allowed to shower to remove the indicator powder.

Study cohort. This study is a retrospective review of TST data from 89 tests of 87 unique individuals referred for clinical testing. The Office of Research Integrity and Compliance reviewed the study and determined that it is exempt from institutional review board review based on US Federal policy 45 CFR 46.101(b) (4). The average age at the time of testing was 14.1 yr old (range 4.8 to 43.2 yr; standard deviation: 5.3), with 28 male patients and 59 female patients. Referral conditions included fatigue or autonomic dysfunction (30 patients); orthostatic complaints such as dizziness or syncope (21); neuropathy or paresthesias (12); abdominal pain, nausea, or vomiting (11); diffuse pain (10); and other conditions (3).

Traditional protocol with novel analysis by color-change powder. In preparing the TST clinical report, the traditional protocol requires a trained technologist to manually record sweating and nonsweating areas on a schematic body outline using a digital paint program to normalize postheating images (Fig. 2) from digital cameras mounted on the ceiling of the thermoregulatory chamber. Our novel encoding method allows semi-automated objective classification of wet and dry

regions over the skin surface without this manual (and subjective) process. In the Lurie Children's Hospital protocol, regions of interest within the pre- and postheating images are defined using the ImageJ Java-based image processing application as follows: a single region following the outline of the body; excluded regions defining unobserved areas; and a small number of example regions outlining nonsweating areas (both before and after heating), along with wet areas defined by a purple shift in the indicator dye (Fig. 2, *A* and *B*). The example regions are then used to train a linear classifier to encode wet and dry regions on a pixel-by-pixel basis (Fig. 2*C*) within the body outline and exclude the unobserved (covered) regions (shown in gray in Fig. 2*D*). The final image is then used to calculate percent anhidrosis over the observed area as the number of "dry" pixels divided by the combined total of "wet" and "dry" pixels. The percent anhidrosis measure, along with the encoded image, is used for clinical reporting.

Comparison of novel analysis by color-change powder with infrared images. For the purposes of the current study, these wet/dry encoded images were compared with images taken from a ceiling-mounted infrared camera. Because the location and optics of this camera (above umbilicus) differed from the visible light cameras (above head and feet) used for color change classification, a method of approximately reconciling these images was developed. Anatomical landmarks in the visible light and infrared images were used to manually define 29 skin surface regions for visible light and infrared images. For example, arms and legs were divided into proximal and distal segments at the elbows and knees. These were further subdivided into medial and lateral areas. The torso was similarly divided laterally and along the sagittal plane. To supplement this coarse-grained analysis using relatively large skin surface regions, an automated method (custom script in MATLAB) was used to geometrically subdivide these manually defined regions into corresponding smaller areas (Fig. 3, *B* and *C*). Because of geometric complexity, left and right hands, and two regions that included irregular exclusion areas for skin surface temperature probes (forehead and lateral right leg), were not further subdivided.

Using the standard indicator powder method, skin surface sweat distributions were determined algorithmically from a sample of wet and dry regions for each patient. To analyze the usefulness of thermal imaging of forced evaporative cooling as an alternative method, spatially localized sweat patterns as determined by the change in color of the indicator was compared with skin surface temperature changes

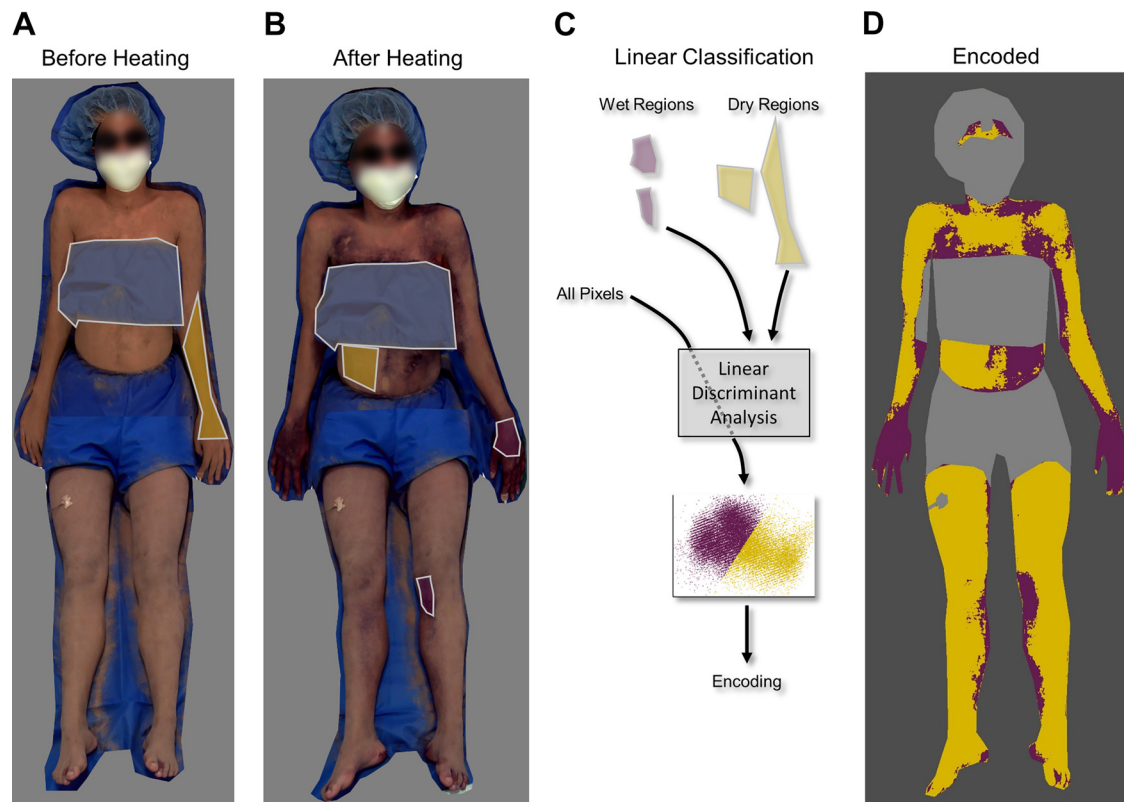


Fig. 2. Semi-automatic classification of skin surface sweating. Images before (A) and after (B) heating used to define outline, covered areas (gray), and example areas of sweating (wet, purple) or nonsweating (dry, yellow). Example regions are used to train a linear discriminant classifier (C), from which all pixels in the image are encoded as sweating or nonsweating (D).

using a method of geometrically subdividing corresponding anatomical regions.

In this way, thermal images and wet/dry coded visible light images taken from different angles could be compared and reconciled to determine the relationship between skin surface evaporative cooling and sweat distribution during the test. The proportion of pixels within each subregion classified as “wet” was calculated along with the mean temperature within the corresponding region in the thermal images. An example of the relationship between skin temperature and the wet proportion is shown in Fig. 3D, where the correlation coefficient is -0.78 [confidence interval (CI): -0.84 to -0.71 ; significance based on 10,000 bootstrap samples, $\alpha = 0.05$]. To examine further the ability of the temperature profile to act as a proxy for the indicator powder, a receiver operating characteristic curve (ROC) was calculated for each test. The ROC curve characterizes the trade-off between sensitivity and specificity in correctly classifying an observation along the range of possible thresholds. In this case, the range of temperature thresholds used to define wet/dry regions is scanned, and the true positive rate (proportion of regions designated as wet by both the thermal and color analyses) and false positive rate (those incorrectly identified as wet from thermal analysis) are calculated. This analysis (as exemplified in Fig. 3E) produces a line within the $[0,1]$ domain where good classification accuracy is characterized by a curve arcing up and to the left. Integrating the area under the curve provides a single metric of accuracy in binary classification problems. In this figure example, the area under the curve is 0.922 (CI: 0.888 to 0.956).

The region splitting method described above was necessary to reconcile visible light images taken with one set of cameras with images from the infrared camera with different placement and optics. It was also needed to be able to match and compare infrared images before fan cooling with those after fan cooling even if the patient

moved. In the absence of patient movement, a much simpler image subtraction method would show the topography of cooling across the skin surface. To estimate the limits of such a method, a series of infrared images were analyzed frame by frame as a subtraction from a baseline image. Each image therefore quantified the temperature change caused by evaporative cooling as the fan airflow passed over the patient’s body. Six regions of sweating and nonsweating were identified from the corresponding indicator powder image, and temperature changes over those regions were calculated for 4 infrared video frames (2 s).

RESULTS

ROC curves for all $n = 89$ patients are shown in Fig. 3. Analyses correlating thermal images and wet/dry encoded visible light images were calculated from thermal images before fan cooling (Fig. 4A), after fan cooling (Fig. 4B), and from the region-by-region difference of pre- and postcooling thermal images (Fig. 4C). On average, analysis using postcooling thermal images was more accurate than the other methods (Fig. 4D), although the method using the difference between pre- and postcooling thermal images was nearly as accurate. For the postcooling analysis, the median area under the ROC curve was 0.837 (CI: 0.816 to 0.86), with no clear relationship to age (Fig. 5A). The median of the best-discriminating temperature was 40.9°C (first to third quartile: 40.2° to 42.1°C ; Fig. 5B).

Composite analyses of thermal and wet/dry encoded visible light images were compiled to illustrate spatial distributions over the body surface across all patients (Fig. 5, C–E). Sweat-

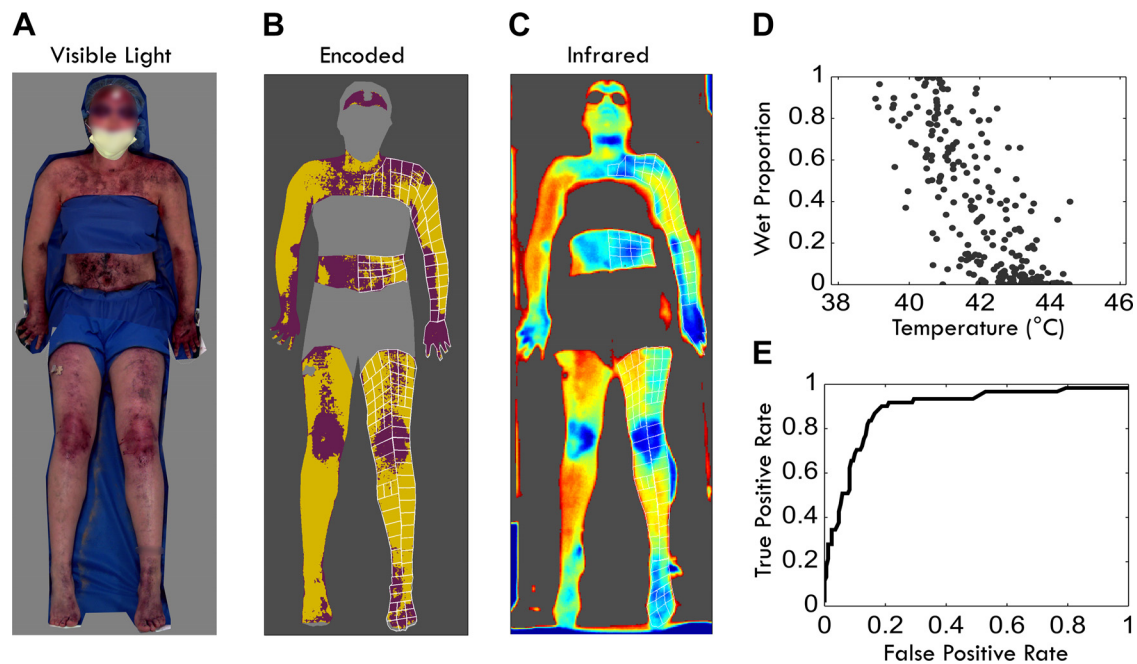


Fig. 3. Example of visible light dye encoded diaphoresis with infrared imaging after forced evaporative cooling. Composite visible light image (A) with areas of purple indicating local sweating, encoding of this sweat distribution with a semiautomatic algorithm (B), and infrared image after fan cooling (C). Sampled regions over the body surface show a negative correlation (D) between fan-cooled skin temperature and encoded pattern of diaphoresis. The accuracy of classifying regions under a given temperature threshold as wet over a range of thresholds is depicted in a receiver operating characteristic curve (E).

ing was most commonly found on the forehead, hands, medial forearms, and, to a lesser extent, the upper torso (Fig. 5C), whereas on average anhidrosis was seen more often along distal (and some proximal) leg areas. The average temperature distribution image shows a corresponding pattern, with cooler measurements recorded in areas that were on average associ-

ated with sweating (Fig. 5D). There was a bilateral difference in surface temperatures with hotter temperatures along the right side, possibly because of less effective fan cooling on that side. To address the possibility of an uneven distribution of cooler temperatures as an indication of sweating, the average correlation coefficient over all observed areas was calculated

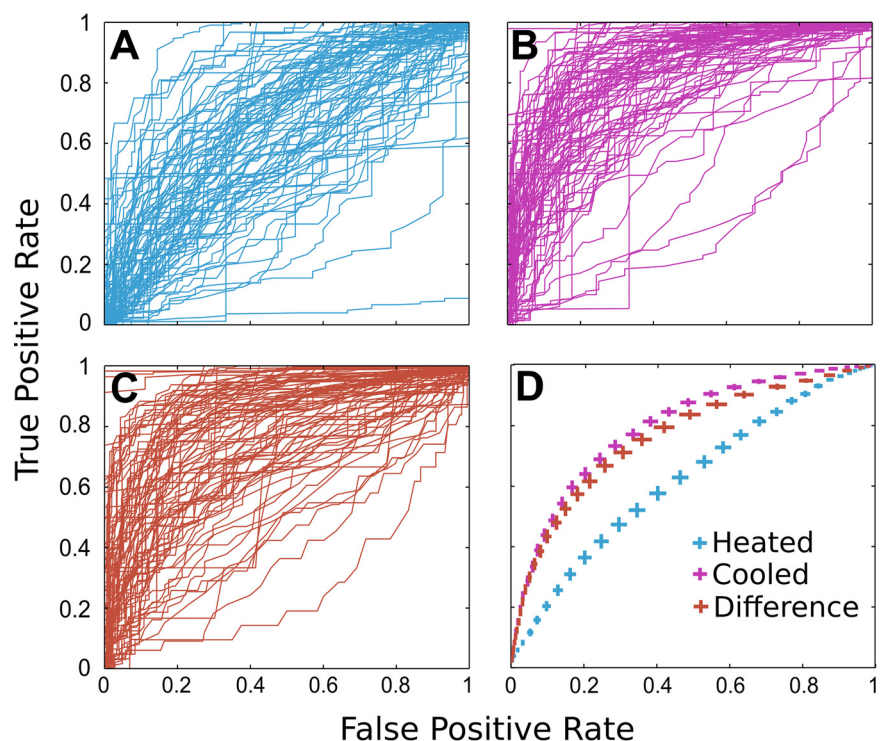


Fig. 4. Receiver operating characteristic (ROC) classification curves for using thermal imaging to identify sweating in all patients at time of maximal heating (A), after cooling (B), and for the region by region difference in temperature during fan cooling (C). Average ROC curves across patients for each method (D) with marker colors matched from A, B, and C (vertical marker length indicates standard error of the mean).

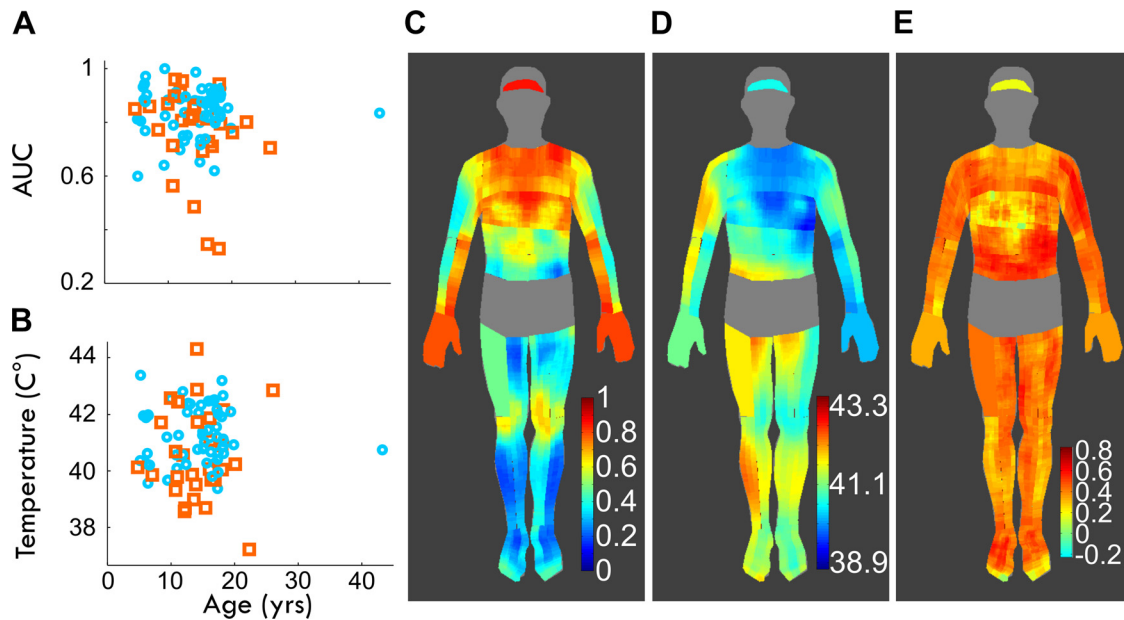


Fig. 5. Accuracy and consistency of correlations between indicator powder- and thermography-derived results across all patients. Receiver operating characteristic area under the curve (AUC, *A*) as a function of age (female patients, orange; male patients, cyan). Threshold temperatures (*B*) producing the best classification accuracy. Sweat distribution likelihood normalized to a schematic body figure (*C*; scale: probability), mean spatial distribution of skin temperature (*D*; scale: °C), and spatial correlation between sweating and cooling (*E*; scale: as positive correlation coefficient).

(shown as a positive correlation in Fig. 5*E*), showing a relatively uniform accuracy across the body surface.

Frame-by-frame analysis of one patient using the image subtraction method (Fig. 6) shows that under direct airflow, sweating regions of skin drop $\sim 0.5^{\circ}\text{C}$ within the first second of cooling, whereas dry regions typically decrease less than 0.25°C (Fig. 6*C*).

DISCUSSION

In contrast to other peripheral nervous system testing modalities, TST provides a means of assessing sudomotor function along the entire neural axis from the central nervous system through peripheral small nerve fibers, which provide sympathetic control over sweat gland function (12). Q-SWEAT is relatively noninvasive but tests only small areas of the body surface, provides information only about peripheral innervation and the sweat glands, and is not well suited to testing the most distally innervated portions of the feet and toes (20). Sympathetic skin responses are not easily graded, tending to be produced in an “all or none” fashion and habituating quickly with repetition (25). Epidermal nerve fiber density estimation, performed via skin biopsy at multiple sites, can quantify innervation with small fibers. However, this method has not been quantified or normed in children, is invasive when done once, and is more invasive with serial measurements (23). Corneal nerve fiber measurements are less invasive but require special expertise and equipment to obtain the images (6).

TST reveals abnormalities of small sensory and autonomic nerve fiber function, which cannot be assessed through standard sensory nerve conduction studies as performed in clinical neurophysiology laboratories. Clinical disorders with neuropathology that can be limited to small nerve fiber dysfunction include complex regional pain syndrome (2), diabetic neuropathy, erythromelalgia (10), multiple system atrophy (21), and

autonomic failure (9). Furthermore, patterns of altered sweating can help identify distal neuropathies and localize pathology to affected spinal nerve roots or peripheral nerves.

TST has been applied successfully in patients as young as 2 yr of age and provided reliable diagnostic data in 98% of 110 children under 16 yr of age studied at Mayo Clinic Rochester (17). However, limitations of the indicator powder method may prevent widespread adoption of this method for use in early diagnosis of neuropathy or other disorders, particularly in pediatrics. Imprecision in the manual application of the powder restricts quantitative analysis. The TST method requires a patient to lie still for up to an hour to keep from disturbing the pattern of the powder. Once testing is finished, the powder can be difficult to completely clean from the skin and can stain clothing if not thoroughly removed (19). Spatial resolution is good, but local quantitative sweat measurement is not possible. Though reactions to the powder are rare, an abundance of caution requires avoiding ingestion, inhalation, or contact with the eyes, meaning that facial sweating is difficult to assess with this method. Furthermore, the length of heat exposure required may be particularly noxious to patients with disorders such as complex regional pain syndrome who may nonetheless benefit from objective and quantitative appraisal. Cumulatively, these difficulties limit the use of this cumbersome, and somewhat uncomfortable, technique in younger and less cooperative patients.

The current standard TST reporting method requires a tedious manual and interpretive process to represent regions of color change on a patient photograph as a distribution of pixels on a normalized digital image representing a schematic body shape. This allows quantification of anhidrosis as a ratio of the number of pixels encoded as dry to those composing the whole body schematic. Although the calculation of this ratio itself is quantitative, the encoding process requires continuous series of

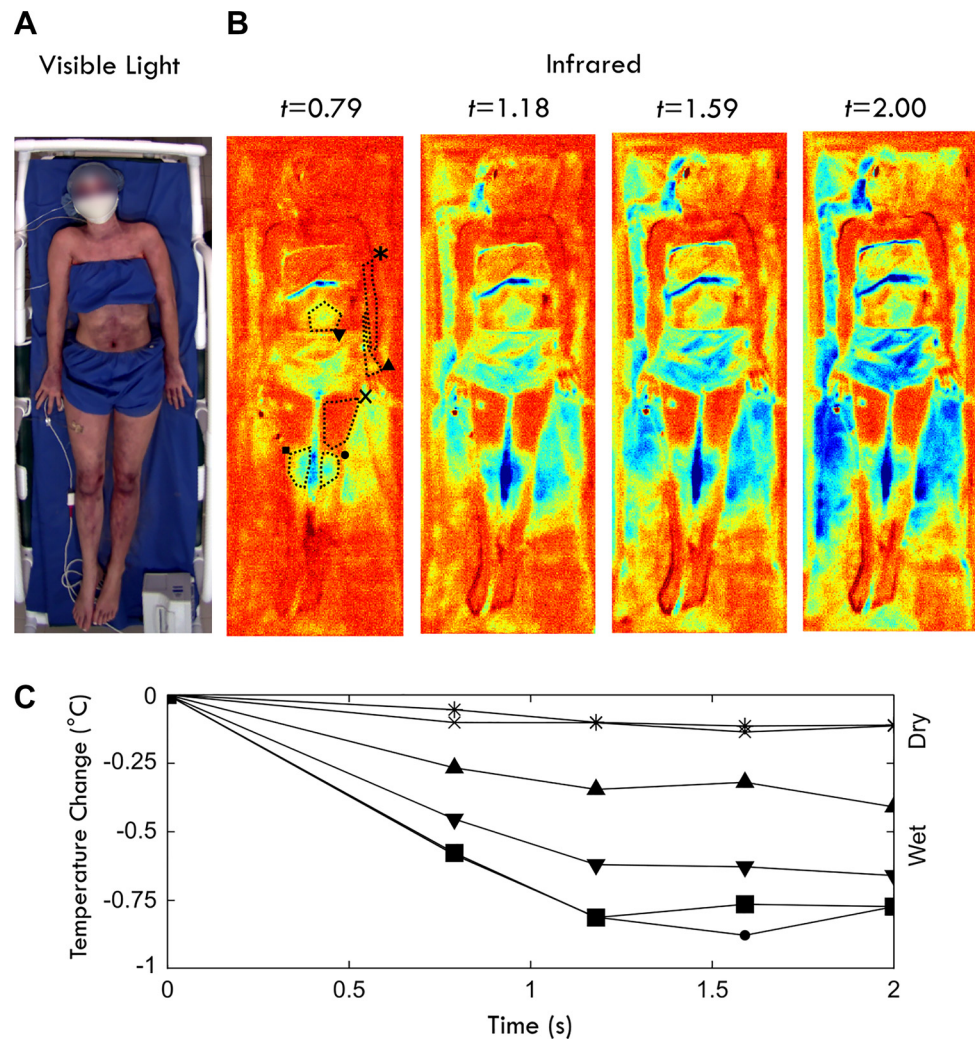


Fig. 6. Temperature changes with fan cooling during high speed thermal imaging in a representative patient. Visible light image (A) and sequential infrared difference images during fan cooling (B) with six anatomic regions of interest (shown for $t = 0.79$ s with markers matched to C). As indicated by purple regions in A, two dry and four sweating regions are shown. Sweating regions show a distinct temperature drop within 1 s of fan cooling (C). Wet regions are the abdomen (\blacktriangledown), left knee (\bullet), right knee (\blacksquare), and medial left forearm (\blacktriangle). Dry regions are the left thigh (\times) and lateral left arm (*).

subjective evaluations. Our semi-automated method, on the other hand, minimizes the interpretive input of the technologist by requiring only the identification of a few exemplar regions representing the most unambiguously wet or dry areas. Thus, this method of encoding images using the traditional indicator powder could make the localization of sweating body surface regions more accurate and objective, with less dependence on individual interpretation. This method has been used successfully in our clinical practice for several years to illustrate patterns of sweating and calculate a global measure of anhidrosis. Although this approach constitutes an important incremental improvement in current practice, it does not alleviate many of the intrinsic difficulties of the indicator powder method that prevent its wider adoption. A more fundamental improvement in current practice, using an infrared camera system, could eliminate the need for the indicator powder altogether. In this study, we have shown that body surface temperature changes produced by forced evaporative cooling correspond closely to regions identified as sweating using the indicator powder. The infrared imaging method produces adequate spatial resolution for clinical purposes and may confer several distinct advantages over the current method using indicator powder. First, thermal imaging eliminates the variability inherent in application of the indicator powder, allowing a potentially more

quantitative assessment of local sweating. The sensitivity of this imaging modality may also allow for faster, less burdensome testing by measuring evaporative temperature loss from small volumes of sweat. In addition, though not specifically addressed in this study, thermal imaging may offer a method to simultaneously test sudomotor and vasomotor function within the same protocol. Although the application of thermography here is novel in that it measures sweat patterns from forced evaporative heat loss, infrared imaging has been described for some time as a tool for characterizing vasomotor or sudomotor function in healthy human physiology (7), both at rest and in thermodynamically stressed conditions (1, 3–5, 8, 11, 14, 16, 18, 24, 26, 27).

Because this study was a retrospective analysis of data incidental to clinical practice, several limitations should be considered. First, the sampled population may not be representative of that seen in other contexts, nor did we have an opportunity to test our method with a population of healthy controls. Nonetheless, although the underlying neuropathologies (or lack thereof) may differ in other settings, we consider it unlikely that the chemical and physical mechanisms that relate skin surface sweat to indicator powder color change, or to evaporative cooling, would differ depending on these underlying conditions. Still, it is possible (indeed likely) that the

evaporative cooling method presented here may be differentially sensitive to sweat volume in ways that may render it more or less applicable to different disorders. Another potential limitation of our use of an existing clinical protocol is that it was not designed to test the limits of infrared imaging in detecting skin surface sweating. However, a close analysis of a representative example infrared video shows that with fast air flow, the temperature difference between sweating and non-sweating regions appears within 1 s of fan cooling. This suggests that, with an optimized cooling and imaging system, sweat patterns could be characterized very quickly, at least in older patients who could follow instructions to hold still. This imaging modality may also be more sensitive than the current method for small amounts of sweat, allowing for a shorter testing protocol overall. Although encouraging, the correlations shown here between fan cooling and indicator powder sweat-coded imaging were not perfect. In several patients, region-by-region classification of cooling as characterized by the area under the ROC curve was smaller than would be expected by chance. These cases tended to be those in which there was either a complete absence of sweating or copious global sweating, indicating that the classification algorithm may need to be adjusted to perform more accurately in these extreme cases. Another source of error seemed to be in encodings of regions that had once sweat and subsequently dried during testing. Although these regions show a light shade of purple with the indicator powder testing, they may be missed by the infrared evaporative cooling method. It is likely that a more consistent and refined protocol would prove faster, more sensitive, and more accurate than the approach described here. For example, instead of a handheld fan, relay control ceiling fans could produce a more homogeneous and reproducible cooling effect. It is also possible that a method using intermittent heating and fan cooling could identify regions of transitory sweating that are captured by the indicator powder method but presumably missed by the single cooling cycle approach we used in this study.

In conclusion, faster, more objective, more quantitative, and less cumbersome measurement of sudomotor function could pave the way for more widespread use of these tests, improving detection, assessment, and treatment for a number of neurologic disorders affecting sudomotor and/or small nerve fiber function. Ultimately, additional research will be needed to validate the infrared evaporative cooling method and allow for a transition of TST to a completely powderless process to improve patient tolerance and drive more widespread adoption. Until then, our results suggest that the current protocol could be made more reproducible and objective with the use of a standard statistical technique.

ACKNOWLEDGMENTS

We thank Dr. Robert Fealey for patient guidance and inspiration in designing the thermoregulatory chamber and modifying clinical methodology.

GRANTS

Research reported in this publication was supported, in part, by the Robert Louis Katz Summer Scholarship Program, the National Institutes of Health's National Center for Advancing Translational Sciences (Grant UL1TR001422), and the Chicago Community Trust Foundation *PHOX2B* Patent Fund.

DISCLOSURES

No conflicts of interest, financial or otherwise, are declared by the authors.

AUTHOR CONTRIBUTIONS

M.S.C. conceived and designed research; D.W.R. performed experiments; M.S.C. and D.W.R. analyzed data; M.S.C., D.W.R., N.L.K., and D.E.W.-M. interpreted results of experiments; M.S.C. prepared figures; M.S.C., N.L.K., and D.E.W.-M. drafted manuscript; M.S.C., N.L.K., and D.E.W.-M. edited and revised manuscript; M.S.C., D.W.R., N.L.K., and D.E.W.-M. approved final version of manuscript.

REFERENCES

1. Barnes RB. Diagnostic thermography. *Appl Opt* 7: 1673–1685, 1968. doi:10.1364/AO.7.001673.
2. Birklein F, Riedl B, Claus D, Neundörfer B. Pattern of autonomic dysfunction in time course of complex regional pain syndrome. *Clin Auton Res* 8: 79–85, 1998. doi:10.1007/BF02267817.
3. Birklein F, Sittl R, Spitzer A, Claus D, Neundörfer B, Handwerker HO. Sudomotor function in sympathetic reflex dystrophy. *Pain* 69: 49–54, 1997. doi:10.1016/S0304-3959(96)03242-3.
4. Bouzida N, Bendada A, Maldague XP. Visualization of body thermoregulation by infrared imaging. *J Therm Biol* 34: 120–126, 2009. doi:10.1016/j.jtherbio.2008.11.008.
5. Brelsford KL, Uematsu S. Thermographic presentation of cutaneous sensory and vasomotor activity in the injured peripheral nerve. *J Neurosurg* 62: 711–715, 1985. doi:10.3171/jns.1985.62.5.0711.
6. Bucher F, Schneider C, Blau T, Cursiefen C, Fink GR, Lehmann HC, Heindl LM. Small-fiber neuropathy is associated with corneal nerve and dendritic cell alterations: an in vivo confocal microscopy study. *Cornea* 34: 1114–1119, 2015. doi:10.1097/ICO.0000000000000535.
7. Clark RP. Human skin temperature and its relevance in physiology and clinical assessment. In *Recent Advances in Medical Thermology*, edited by Ring EFJ, Phillips B. Boston, MA: Springer New York, 1984, p. 5–15. doi:10.1007/978-1-4684-7697-2_2.
8. Clark RP, Mullan BJ, Pugh LG. Skin temperature during running—a study using infra-red colour thermography. *J Physiol* 267: 53–62, 1977. doi:10.1113/jphysiol.1977.sp011800.
9. Cohen J, Low P, Fealey R, Sheps S, Jiang NS. Somatic and autonomic function in progressive autonomic failure and multiple system atrophy. *Ann Neurol* 22: 692–699, 1987. doi:10.1002/ana.410220604.
10. Davis MD, Genebriera J, Sandroni P, Fealey RD. Thermoregulatory sweat testing in patients with erythromelalgia. *Arch Dermatol* 142: 1583–1588, 2006. doi:10.1001/archderm.142.12.1583.
11. Deng ZS, Liu J. Enhancement of thermal diagnostics on tumors underneath the skin by induced evaporation. *Conf Proc IEEE Eng Med Biol Soc* 7: 7525–7528, 2005. doi:10.1109/IEMBS.2005.1616253.
12. Fealey R. Thermoregulatory sweat test (3rd ed.). In: *Clinical Autonomic Disorders*. Baltimore, MD: Lippincott Williams & Wilkins, 2008, p. 244–260.
13. Fealey R. Thermoregulatory sweat test (2nd ed.). In: *Clinical Autonomic Disorders*. Philadelphia, PA: Lippincott-Raven, 1997, p. 245–257.
14. Fushimi H, Inoue T, Nishikawa M, Matsuyama Y, Kitagawa J. A new index of autonomic neuropathy in diabetes mellitus: heat stimulated thermographic patterns. *Diabetes Res Clin Pract* 1: 103–107, 1985. doi:10.1016/S0168-8227(85)80035-8.
15. Guttman L. The management of the quinizarin sweat test (Q.S.T.). *Postgrad Med J* 23: 353–366, 1947. doi:10.1136/pgmj.23.262.353.
16. Huygen FJ, Niehof S, Klein J, Zijlstra FJ. Computer-assisted skin videothermography is a highly sensitive quality tool in the diagnosis and monitoring of complex regional pain syndrome type I. *Eur J Appl Physiol* 91: 516–524, 2004. doi:10.1007/s00421-003-1037-6.
17. Kuntz NL, Hemenway KL, Fealey RD. Utility of diagnostic thermoregulatory sweat test in children. In: *Neurology*. Philadelphia, PA: Lippincott Williams & Wilkins, 2011, p. A575–A575.
18. Lahiri BB, Bagavathiappan S, Jayakumar T, Philip J. Medical applications of infrared thermography: a review. *Infrared Phys Technol* 55: 221–235, 2012. doi:10.1016/j.infrared.2012.03.007.
19. Low PA. Testing the autonomic nervous system. *Semin Neurol* 23: 407–421, 2003. doi:10.1055/s-2004-817725.
20. Low PA, Caskey PE, Tuck RR, Fealey RD, Dyck PJ. Quantitative sudomotor axon reflex test in normal and neuropathic subjects. *Ann Neurol* 14: 573–580, 1983. doi:10.1002/ana.410140513.
21. Low PA, Tomalia VA, Park KJ. Autonomic function tests: some clinical applications. *J Clin Neurol* 9: 1–8, 2013. doi:10.3988/jcn.2013.9.1.1.

22. **Low PA, Walsh JC, Huang CY, McLeod JG.** The sympathetic nervous system in diabetic neuropathy. A clinical and pathological study. *Brain* 98: 341–356, 1975. doi:[10.1093/brain/98.3.341](https://doi.org/10.1093/brain/98.3.341).
23. **Provitera V, Gibbons CH, Wendelschafer-Crabb G, Donadio V, Vitale DF, Stancanelli A, Caporaso G, Liguori R, Wang N, Santoro L, Kennedy WR, Nolano M.** A multi-center, multinational age- and gender-adjusted normative dataset for immunofluorescent intraepidermal nerve fiber density at the distal leg. *Eur J Neurol* 23: 333–338, 2016. doi:[10.1111/ene.12842](https://doi.org/10.1111/ene.12842).
24. **Saxena AK, Willital GH.** Infrared thermography: experience from a decade of pediatric imaging. *Eur J Pediatr* 167: 757–764, 2008. doi:[10.1007/s00431-007-0583-z](https://doi.org/10.1007/s00431-007-0583-z).
25. **Shahani BT, Halperin JJ, Boulu P, Cohen J.** Sympathetic skin response—a method of assessing unmyelinated axon dysfunction in peripheral neuropathies. *J Neurol Neurosurg Psychiatry* 47: 536–542, 1984. doi:[10.1136/jnnp.47.5.536](https://doi.org/10.1136/jnnp.47.5.536).
26. **Sun PC, Lin HD, Jao SH, Chan RC, Kao MJ, Cheng CK.** Thermoregulatory sudomotor dysfunction and diabetic neuropathy develop in parallel in at-risk feet. *Diabet Med* 25: 413–418, 2008. doi:[10.1111/j.1464-5491.2008.02395.x](https://doi.org/10.1111/j.1464-5491.2008.02395.x).
27. **Torii M, Yamasaki M, Sasaki T, Nakayama H.** Fall in skin temperature of exercising man. *Br J Sports Med* 26: 29–32, 1992. doi:[10.1136/bjism.26.1.29](https://doi.org/10.1136/bjism.26.1.29).

